Practical strategies for interbed multiple attenuation

Gaurav Dutta*, Hui Huang, Karthik Kanakamedala, Bin Deng, and Ping Wang, CGG

Summary

Interbed multiples cause artifacts in subsurface images because they are incorrectly migrated when using standard primary-based migration algorithms. While surface-related multiple elimination has been well established as a standard step in seismic processing, the usage of interbed multiple attenuation (IMA) remains low due to various practical challenges, such as inaccuracy in prediction, difficulty in subtraction, and prohibitively high compute cost. We propose a workflow with a few strategies to improve the applicability of IMA. Using a 3D field data example, we demonstrate the effectiveness of our workflow in predicting and attenuating interbed multiples.

Introduction

Interbed multiple attenuation (IMA) is one of the most challenging steps in seismic processing. In some cases, these multiples strongly interfere with primaries and have been shown to affect the interpretation of hydrocarbon reservoirs (Griffiths et al., 2011; Hembd et al., 2011; Cypriano et al., 2015). Unlike surface-related multiple elimination (SRME) (Verschuur et al., 1992), which is a standard step in seismic processing, the usage of IMA remains low for several reasons. First, the cost has been prohibitive for production-size 3D data sets since a typical implementation of IMA is, by nature, around two to three orders of magnitude more computationally expensive than SRME. Coarse integration grids and small apertures have to be used for IMA in order to complete it in a reasonable time, which often leads to downgraded model quality. Second, subtraction of the interbed multiples from the input data is challenging because of their relatively weak amplitudes and strong event interference with the primary signals.

The Jakubowicz (1998) approach has long served as the main prediction algorithm for interbed multiples. The method is based on the convolution and cross-correlation of three wavefield components that are obtained by windowing the data around user-specified horizons that act as upgoing and downgoing generators for the incoming wavefields. The convolution and cross-correlation operations require an integration of the recorded wavefields over a 4D user-specified aperture, compared to a 2D aperture in the SRME case. The need for layer-stripping to account for different multiple generators makes the whole prediction process infeasible for modern-day production data sets. Other approaches, such as using an inverse scattering series derived from the Lippmann-Schwinger equation (Weglein et al., 1997) and layer-based approaches (Verschuur and Berkhout, 2005; Pica and Delmas, 2008) have also been

explored in the context of IMA. However, some of these approaches are model-driven and usually require several rounds of migration-demigration of the input data. These methods are also as expensive as that of Jakubowicz (1998).

Inspired by the Marchenko-based redatuming workflow proposed by van der Neut and Wapenaar (2016), Pereira et al. (2018) modify the interbed multiple prediction approach of Jakubowicz (1998) by first executing the cross-correlation operator to generate a virtual data set. In the next step, the convolution between the original data and the virtual data is computed to generate the interbed multiple model. Conceptually, this two-step approach is equivalent in cost to two SRMEs and thus is much faster than the simultaneous convolution-cross-correlation IMA workflow. The success of this approach relies on an accurate generation of the virtual data that have to be computed on an extended area that is much larger than the original prediction area and usually with a denser spatial sampling. For industrial problems, the generation of the virtual data alone can be around 20-40 times slower than SRME. It is still crucial to further reduce the compute cost of this IMA approach, especially the first step, for it to be widely adopted for large-scale field data sets.

For our workflow, we combined the Jakubowicz (1998) method and the two-step strategy (van der Neut and Wapenaar, 2016; Pereira et al., 2018). Since both ends of the middle trace used for cross-correlation fall on regular grids, this can be used to further reduce the compute cost. Thus, the middle traces and traces from the same shot and receiver locations, once computed, can be reused by neighboring shots and/or receivers, which effectively reduces the duplicated computation. In addition, we propose a post-migration curvelet-domain subtraction for better discrimination of interbed multiples and better frequency and dip separation of primaries and interbed multiples. The Santos Basin in offshore Brazil is a good candidate for our workflow, as stratified salt layers, the water bottom, the top and base of salt bodies, the top of Cretaceous and Albian formations and the presence of volcanic rocks can all act as potential generators of interbed multiples (Meisling et al., 2001; Krueger et al., 2018). We use a 3D field data example from this basin to validate our proposed method.

Method

Figure 1 represents the schematic for interbed multiple prediction. For a source at S and a receiver at R, the interbed multiple between S and R can be predicted as
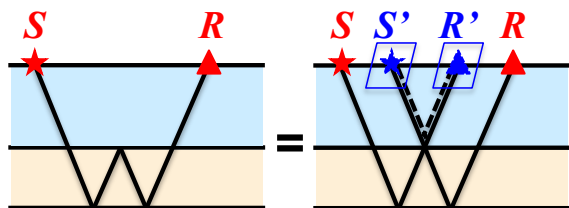
Figure 1: Schematic for interbed multiple prediction (Jakubowicz, 1998). The interbed multiple between a source at S and a receiver at R is calculated by convolving a trace SR' with another trace $S'R$ and then cross-correlating with a third trace $S'R'$. The two blue boxes indicate the 2D integration apertures around S' and R', respectively. These two 2D integrations effectively lead to a 4D integration.
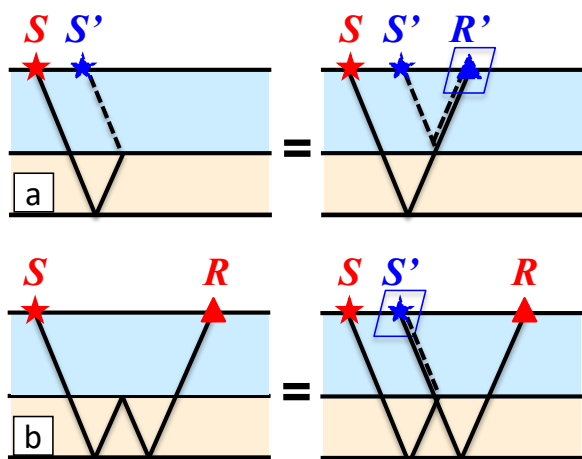

Figure 2: Schematic for reducing the 4D integration in Equation 1a to two sequential 2D integrations. The virtual shot $V(S, S')$ is first computed by executing the cross-correlation step in Equation 1b (a). Once $V(S, S')$ is computed, these virtual shots are convolved with real-receiver gathers $G(S', R)$ by reusing the same virtual traces for neighboring real-receiver locations on the surface (b).

$$G(S,R) = \int_{S'} \int_{R'} G(S,R')G(S',R)G^*(S',R') \, dR' \, dS' \quad (1a)$$
$$= \int_{S'} \left[\int_{R'} G(S,R')G^*(S',R') \, dR' \right] G(S,R) \, dS' \quad (1b)$$
$$= \int_{S'} \underbrace{V(S,S')}_{Virtual\ Shot} G(S',R) dS' \quad , \quad (1c)$$

where $G(S,R)$ represents the band-limited frequency-domain Green's function recorded for a source at S and a receiver at R and $*$ represents complex conjugation. For ease of representation, the wavelet and frequency-dependent terms have been omitted. Equation 1a represents a 4D integration over the source- and receiver-side apertures S' and R', respectively (shown by the blue boxes in Figure 1). When compared with SRME, which involves only a single convolution operation, the apparent computational cost of the multiple prediction operation based on simultaneous convolution and cross-correlation is at least two orders of magnitude more expensive than SRME.
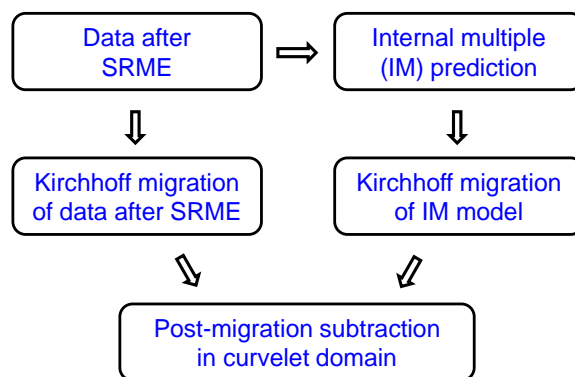

Figure 3: IMA prediction and adaptive subtraction flow.

The 4D integration in Equation 1a can be reduced to two sequential 2D integrations. This is done by first executing the cross-correlation operation, as shown in Equation 1b, to generate virtual shot gathers $V(S, S')$. In this step, the integration is carried out over the 2D virtual-receiver locations R' on the recording surface (Figure 2a). The virtual shot S' has a denser and wider distribution than the receiver sampling of the naturally acquired seismic data. In addition, to generate high-quality virtual shot gathers, a denser integration grid over R' may be needed. Therefore, the computational cost for computing $V(S, S')$ can be 20-40 times that of SRME.

To reduce the compute cost of the first step, we exploit the fact that both ends of the trace $S'R'$ fall on regular grids since the locations of these points on the surface are determined by the source-receiver offset and the user-determined integration apertures. This makes it possible to reuse the same middle traces (dashed-line raypath in Figure 2a) and traces from the same shot (solid-line raypath in Figure 2a) for neighboring shots and receivers. The key to this process is to simultaneously handle as many shots and receivers as possible to achieve the maximum reduction of duplicate computation. A similar strategy can be used for the second step during the convolution stage of the prediction using Equation 1c. Since the virtual source location S' also falls on a regular grid, many of the virtual traces can again be reused by neighboring receivers during convolution with the real-receiver gathers $G(S', R)$.

The predicted interbed multiples from our algorithm are then subtracted from the input in the post-migration domain. This is done because unlike surface-related multiples that are clearly evident in the input data in the shot- or channel-domains, interbed multiples are hard to visualize due to relatively weak amplitudes and strong event interference with the primary signals. These events are easier to discriminate against in the post-migration domain, either

using stacked images or pre-stack offset gathers. In addition, the adaptive subtraction is carried out using 3D curvelet-domain subtraction (Wu and Hung, 2015) for better frequency and dip discrimination between primaries and interbed multiples. The full workflow for IMA is shown in Figure 3.

Application to field data

The proposed algorithm was applied to a 3D narrow azimuth data set from the Santos Basin in offshore Brazil, where interbed multiples have been shown to create serious imaging artifacts in the pre-salt reservoirs (Hembd et al., 2011; Cypriano et al., 2015; Krueger et al., 2018). These multiples are generated by the water bottom, top and base of salt, and the stratified salt layers, and directly interfere with the interpretation of the pre-salt reservoirs by providing misleading AVO information. The green arrows in Figure 4a show a strong long-period interbed multiple artifact generated by the water bottom, top of salt, and stratified salt layers in a migrated stack image and surface-offset gathers. The suspected raypath of this multiple is shown using the blue lines in Figure 4a.

The acquisition for this study was done with 12 variable-depth streamers with a depth range of 10-50 m, a cable separation of 100 m, a cable length of 8100 m and a sailline separation of ~600 m. The survey covered an area of approximately 17,500 sq. km. Standard processing steps like denoise, designature, 3D source- and receiver-side deghosting, and SRME were first applied to the data. The target area where the interbed multiples need to be predicted is around the green arrows in Figure 4a. The base of salt horizon was chosen to separate the overburden area containing the IM generators and the target area. Thus, all possible multiples, like the one shown by the blue arrow in Figure 4a, whose source-side upgoing bounce point and the downgoing bounce point fall above the horizon are predicted. The receiver-side reflection can be anywhere in the model (van der Neut and Wapenaar, 2016; Krueger et al., 2018). In the context of Figure 2a, the traces SR' and $S'R'$ were obtained by muting out the data below the base of salt while the receiver-side trace $S'R$ was the recorded data without any mutes.

The stacked migration sections and the pre-stack offset gathers before and after interbed multiple attenuation are
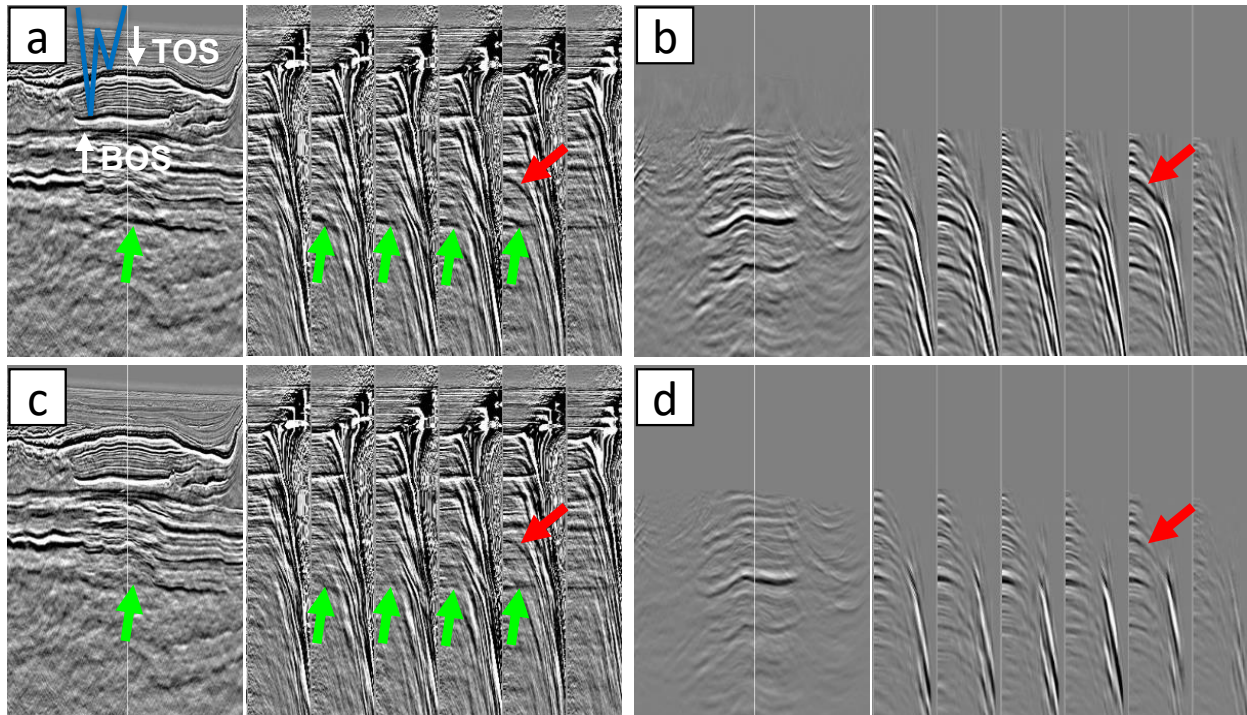

Figure 4: Migrated stack image and surface offset gathers (a) before IMA; (b) interbed multiple model; (c) after IMA; and (d) the difference between (a) and (c). Blue lines indicate the raypath of interbed multiples. The green arrows indicate the interbed multiples that have been largely eliminated after IMA, and the red arrows indicate some short-period interbed multiples that are predicted in the multiple model but not fully subtracted.

shown in Figures 4a-d. It is evident from these figures that the strong imaging artifacts caused by the interbed multiples have been reasonably mitigated and the interpretation of the geology is now less ambiguous. The downward curving events, shown in the offset gathers in Figure 4a, are generated by the interbed multiples present in the data and can be mistaken for real primary events during residual velocity analysis. These events have been largely removed after IMA, as shown in Figure 4c. Figures 4b and 4d indicate a reasonable consistency between the interbed multiples predicted and the ones subtracted out using curvelet-domain adaptive subtraction. Migrated inline and crossline sections in another area of the survey, shown in Figures 5a-d, also indicate the benefits of using IMA. The blue arrows and circles in Figure 5 indicate the pre-salt interbed multiples that have been eliminated after IMA.

Conclusions

We have proposed a few strategies to speed up the prediction of interbed multiples using a fully data-driven workflow. Our proposed algorithm makes it possible to use large apertures and dense integration grids for optimal results during the cross-correlation and convolution stages of the prediction. Even though IMA is still quite expensive, it is applicable to very large production-size data sets by using our workflow. The proposed method has been successfully applied on various 3D field data sets, and the imaging artifacts generated by interbed multiples are largely eliminated for an accurate interpretation of the geology.

Adaptive curvelet-domain subtraction is still preferred for subtracting the interbed multiples in the post-migration domain, which requires an additional migration of the predicted interbed multiples. The proposed approach also requires at least one user-specified horizon, and the prediction of short-period interbed multiples is still a challenge.
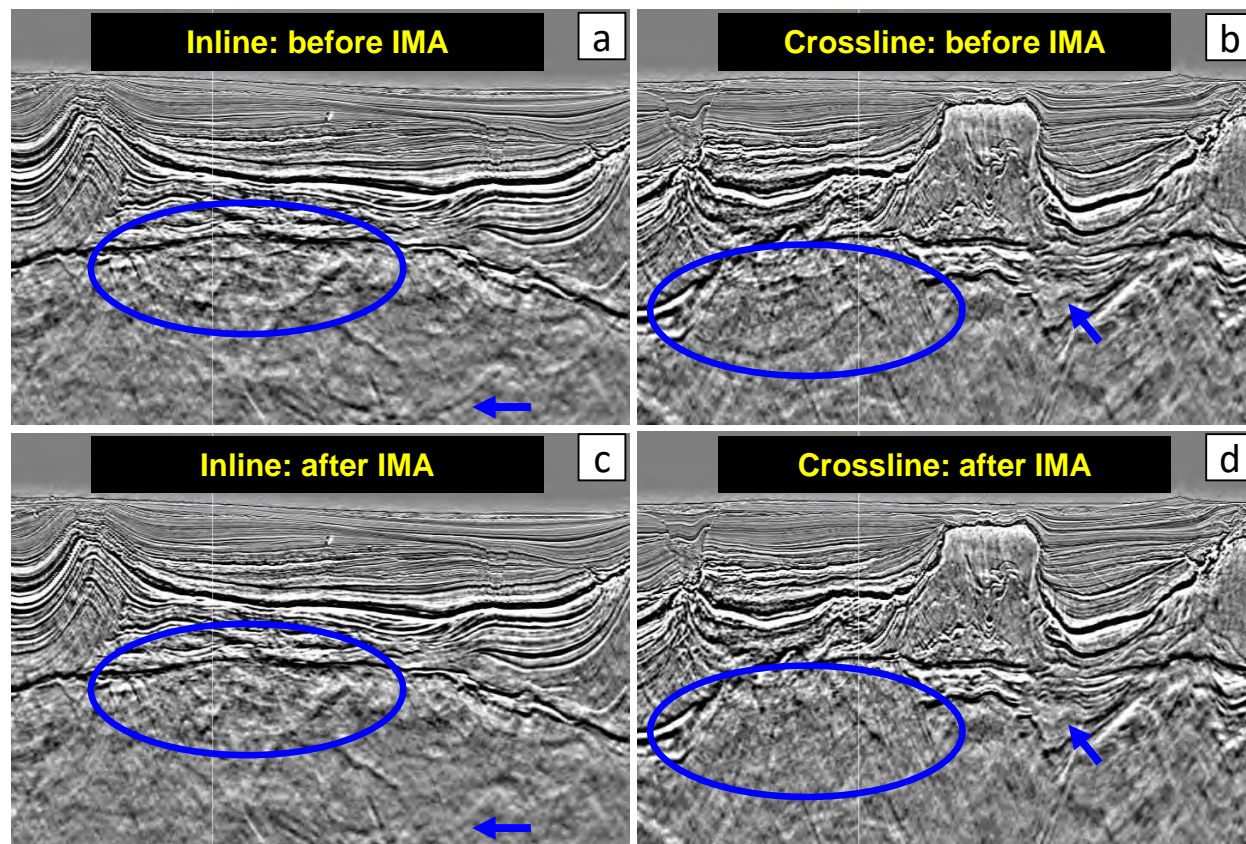
Acknowledgments

Figure 5: Migrated inline/crossline sections (a)/(b) before IMA and (c)/(d) after IMA. The blue arrows and circles show some strong interbed multiples in the pre-salt areas that have been largely eliminated after IMA.

REFERENCES

Cypriano, L., F., Marpeau, R., Brasil, G., Welter, H., Prigent, H., Douma, M., Velasques, J., Boechat, P., de Carvalho, C., Guerra, and C., Theodoro, 2015, The impact of inter-bed multiple attenuation on the imaging of pre-salt targets in the Santos basin off-shore Brazil: 77th Conference and Exhibition, EAGE, Extended Abstracts, Tu N114 06, doi: https://doi.org/10.3997/2214-4609.201412691.

Griffiths, M., J., Hembd, and H., Prigent, 2011, Applications of interbed multiple attenuation: The Leading Edge, **30**, 806–912, doi: https://doi.org/10.1190/1.3626498.

Hembd, J., M., Griffiths, C., Ting, and N., Chazalnoel, 2011, Application of 3D interbed multiple attenuation in the Santos Basin, Brazil: 73rd Conference and Exhibition, EAGE, Extended Abstracts, H047, doi: https://doi.org/10.3997/2214-4609.20149270.

Jakubowicz, H., 1998, Wave equation prediction and removal of interbed multiples: 68th Annual International Meeting, SEG, Expanded Abstracts, 1527–1530, doi: https://doi.org/10.1190/1.1820204.

Krueger, J., D., Donno, R., Pereira, D., Mondini, A., Souza, J., Espinoza, and A., Khalil, 2018, Internal multiple attenuation for four presalt fields in the Santos Basin, Brazil: 88th Annual International Meeting, SEG, Expanded Abstracts, 4523–4527, doi: https://doi.org/10.1190/segam2018-2990024.1.

Meisling, K. E., P. R., Cobbold, and V. S., Mount, 2001, Segmentation of an obliquely rifted margin, Campos and Santos basins, southeastern Brazil: AAPG Bulletin, **85**, 11903–11924, doi: https://doi.org/10.1306/8626D0A9-173B-11D7-8645000102C1865D.

Pereira, R., D., Mondini, and D., Donno, 2018, Efficient 3D internal multiple attenuation in the Santos basin: 80th Conference and Exhibition, EAGE, Extended Abstracts, We C08, doi: https://doi.org/10.3997/2214-4609.201801073.

Pica, A. and L., Delmas, 2008, Wave equation based internal multiple modeling in 3D: 78th Annual International Meeting, SEG, Expanded Abstracts, 2476–2480, doi: https://doi.org/10.1190/1.3063858.

van der Neut, J., and K., Wapenaar, 2016, Adaptive overburden elimination with the multidimensional Marchenko equation: Geophysics, **81**, no. 5, T265–T284, doi: https://doi.org/10.1190/geo2016-0024.1.

Verschuur, D. J., A. J., Berkhout, and C. P. A., Wapenaar, 1992, Adaptive surface-related multiple elimination: Geophysics, **57**, 1166–1177, doi: https://doi.org/10.1190/1.1443330.

Verschuur, D., and A., Berkhout, 2005, Removal of internal multiples with the common-focus-point (CFP) approach — Part 2: Application strategies and data examples: Geophysics, **70**, no. 3, V61–V72, doi: https://doi.org/10.1190/1.1925754.

Weglein, A. B., F. A., Gasparotto, P. M., Carvalho, and R. H., Stolt, 1997, An inverse-scattering series method for attenuating multiples in seismic reflection data: Geophysics, **62**, 1975–1989, doi: https://doi.org/10.1190/1.1444298.

Wu, X., and B., Hung, 2015, High-fidelity adaptive curvelet domain primary-multiple separation: First Break, **33**, 13–59, doi: https://doi.org/10.1071/ASEG2013ab094.